Calculated Equilibrium Composition and Radiation of Metallic Plasmas Produced in Hypervelocity Impact

KENNETH E. HARWELL*
Auburn University, Auburn, Ala.

AND

JAMES L. REID† AND ALBERT R. HUGHES†
Hayes International Corporation, Birmingham, Ala.

The composition equations were derived for a two-element metallic plasma in local thermodynamic equilibrium. Calculations were carried out for aluminum, iron, and aluminum-iron plasmas for pressures of 1, 10, and 100 atm and temperatures of 5000°–40,000°K. Internal partition functions were calculated assuming series terminating quantum numbers determined by applying the Debye shielding criterion. Spectral line radiation, recombination radiation and bremsstrahlung were calculated in an attempt to predict impact flash. The radiated energy was calculated as a function of wavelength and then summed over five wavelength intervals corresponding to filter intervals used in some impact flash experiments. For the aluminum plasma, quantitative agreement between theory and experiment could be obtained only by inferring pressure broadening and line shift. Some qualitative agreement was obtained between the shape of the calculated spectral distribution curve for a pure iron plasma and the experimental distribution curve for iron-iron impacts. For the case of aluminum-iron and iron-aluminum impacts, theoretical spectral distribution curves could be selected that agreed qualitatively with the experimental results.

Introduction

WHEN a hypervelocity projectile impacts a target, part of its kinetic energy is converted into electromagnetic energy which produces the so-called impact flash. Detailed measurements and analysis of the flash can be used as a diagnostic technique to provide information about the velocity,[1] size, and composition[2] of the projectile. MacCormack[3] fired aluminum projectiles at aluminum targets and observed the existence of spectral line radiation. Koehler[4] impacted lead targets with various projectile materials and found that the measured radiation was characterized by excitation of the atoms of the projectile material. Koehler also observed continuum radiation emanating from the impact interface. Jean and Rollins[5] observed line emissions, characteristic of both projectile and target material, as well as continuum radiation. They identified spectral lines that were characteristic of ionized aluminum, cadmium, and magnesium in addition to those of the excited neutral atoms. Jean[6] photographed the flash produced by aluminum-aluminum impacts and found that the radiation appeared to have been emitted from a luminous metallic gas cloud produced at the projectile-target interface (shown schematically in Fig. 1).

The theoretical model reported here assumes that the radiation is emitted from a unit volume containing neutral atoms, heavy positive ions, and electrons in local thermodynamic equilibrium (LTE). In the actual impact event, the plasma created will have spatial gradients in temperature, pressure, and composition, and it probably will not be in equilibrium due to the rapid expansion of radiating gas from the point of impact. However, a complete analysis of such a nonequilibrium plasma would require a detailed knowledge of the specific physical mechanisms and collisions occurring in the radiating volume. Lacking such knowledge, it is reasonable to assume that the actual nonequilibrium event can be described by a succession of LTE states. Thus, although the plasma density and temperature may vary in space and time, the distribution of particles between the various energy states at any instant of time and location in space may depend only on the local values of temperature, density, and chemical composition of the plasma. These properties were assumed to be known or inferred from experimental data. In principle, although experimentally measured radiation intensity data can be Abel-inverted to yield the plasma density variation with spatial location, this has not been accomplished for impact flash data.

The assumption of LTE permits determination of the population densities from the equipartition energy law of statistical mechanics without a quantitative knowledge of the atomic cross sections. For this case, the population of bound energy levels within a given species is described by Maxwell-Boltzmann statistics and the Boltzmann equation. For moderately dense plasmas ($N_e \gtrsim 10^{16}$ cm^{-3}) at moderate temperatures ($T \lesssim 6 \times 10^4$°K), the velocity distribution of free electrons is almost always Maxwellian.[7,8] The relative total populations of successive stages of ionization are given by the mass action or Saha equations.

It is assumed that the distribution functions respond instantly to any change in the plasma conditions and that each collisional process occurs at the same rate as its inverse, so that the principle of detailed balancing is satisfied. Another requirement of the model is that the ions and atoms in the plasma do not diffuse into regions of significantly different electron temperature in the relaxation time required for their level populations to reach equilibrium.[9] For the electron number densities of interest here ($N_e \gtrsim 10^{16}$ cm^{-3}), the electron equilibration times are considerably shorter than the times required for equilibration of the bound energy levels of the atoms and ions. As long as the collisional rates of energy

Received March 31, 1970; revision received November 30, 1970. This research was supported in part by the Air Force Armament Laboratory, Air Force Systems Command, Eglin Air Force Base, under contract F 08(635)-5120.

* Alumni Associate Professor, Aerospace Engineering Department and Consultant, Hayes International Corporation. Associate Member AIAA.

† Research Scientist, Engineering Research Division.

transfer are much higher than the radiative rates of energy transfer, the present LTE model should give reasonable estimates of the energy radiated from an optically thin impact plasma. This radiation was assumed to be one of the following types: 1) line emission due to internal (bound-bound) electronic transitions in the atoms and ions, 2) continuum emission due to electron-ion recombination (free-bound) transitions, and 3) continuum emission (bremsstrahlung) due to electron-ion collisional (free-free) transitions.

Since all three types of emitted radiation depend on free electron, ion, and/or neutral atom number densities, the first step in developing a mathematical model of the impact flash will be to derive equations for the plasma composition as a function of local temperature and pressure. A two-element (species A and B) plasma will be chosen so that the projectile and target materials can be different. Once the composition of the plasma is known, the radiation emitted in the form of line radiation, recombination radiation, and bremsstrahlung will be calculated. The numerical results for aluminum-aluminum, iron-iron, and aluminum-iron impacts will be presented and compared with experimental data to the extent possible.

Local Thermodynamic Equilibrium (LTE) Plasma Composition Model[10]

Charge neutrality requires that

$$N_e = \sum_{i=1}^{N} iN_A(i) + \sum_{j=1}^{M} jN_B(j) \tag{1}$$

where N_e is the electron number density; N and M are the highest degrees of ionization attained for species A and B, respectively; and i and j denote the degree of ionization, i.e., 1 denotes the singly ionized atom, 2 the doubly ionized atom, etc. Conservation of heavy particle number density N_H requires that $N_H = N_A + N_B$ be constant for a given pressure and temperature. Where

$$N_A = \sum_{i=0}^{N} N_A(i) \qquad N_B = \sum_{j=0}^{M} N_B(j) \tag{2}$$

The total number density N_T is given as $N_T = N_H + N_e$. The various number densities of the plasma are related by the mass-action (Saha) equations

$$N_A(i)N_e/N_A(i-1) = K_i = 2(2\pi m_e kT/h^2)^{3/2} \frac{Q_A(i)}{Q_A(i-1)} \exp\{[I_A(i-1) - I_A(i)]/kT\} \tag{3}$$

$$N_B(j)N_e/N_B(j-1) = k_j = 2(2\pi m_e kT/h^2)^{3/2} \frac{Q_B(j)}{Q_B(j-1)} \exp\{[I_B(j-1) - I_B(j)]/kT\} \tag{4}$$

where h is Planck's constant, m_e is the electron mass, k is Boltzmann's constant, T is the temperature, and K_i and k_j are the mass action coefficients for species A and B, respectively. The Q's are the internal partition functions for the two species and the I's are the relevant ionization potentials. Using these relations, the expressions for the number densities become

$$N_A(i) = \frac{N_A(0)}{N_e{}^i} \prod_{r=1}^{i} K(r); \qquad N_B(j) = \frac{N_B(0)}{N_e{}^j} \prod_{r=1}^{j} k(r)$$

The total particle density is then expressed as

$$N_T = N_H + N_e = \alpha N_H \left\{\left[1 + \sum_{i=1}^{N} \frac{i+1}{N_e{}^i} \prod_{r=1}^{i} K(r)\right] \Big/ \left[1 + \sum_{i=1}^{N} \frac{1}{N_e{}^i} \prod_{r=1}^{i} K(r)\right]\right\} + \beta N_A \left\{\left[1 + \sum_{j=1}^{M} \frac{j+1}{N_e{}^j} \prod_{r=1}^{j} k(r)\right] \Big/ \left[1 + \sum_{j=1}^{M} \frac{1}{N_e{}^j} \prod_{r=1}^{j} k(r)\right]\right\} \tag{5}$$

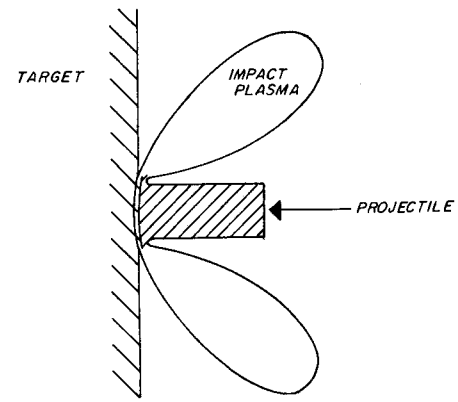

Fig. 1 Schematic representation of impact plasma cloud.

where $\alpha = N_A/N_H$ and $\beta = N_B/N_H$ (such that $\alpha + \beta = 1$) were introduced to permit relative amounts of species A and B to be specified. N_H can be eliminated to yield an electron density polynomial that may be solved for any degree of ionization of species A and B. In the calculation reported here, A was chosen to be 3 whereas B was chosen to be 2. For $N = 3$ and $M = 2$, the following electron density polynomial results:

$$A_1N_e{}^6 + A_2N_e{}^5 + A_3N_e{}^4 + A_4N_e{}^3 + A_5N_e{}^2 + A_6N_e + A_7 = 0 \tag{6}$$

where

$$A_1 = 1,\ A_2 = (1+\alpha)K_1 + (2-\alpha)k_1$$

$$A_3 = (1+2\alpha)K_1K_2 + 2K_1k_1 + (3-2\alpha)k_1k_2 - \alpha N_TK_1 - (1-\alpha)N_Tk_1$$

$$A_4 = (1+3\alpha)K_1K_2K_3 + (2+\alpha)K_1K_2k_1 + (3-\alpha)k_1k_1k_2 - 2\alpha N_TK_1K_2 - N_TK_1k_1 - 2(1-\alpha)N_Tk_1k_2$$

$$A_5 = 2(1+\alpha)K_1K_2K_3k_1 + 3K_1K_2k_1k_2 - 3\alpha N_TK_1K_2K_3 - (2-\alpha)N_TK_1k_1k_2 - (1+\alpha)N_TK_1K_2k_1$$

$$A_6 = (3+\alpha)K_1K_2K_3k_1k_2 - (1+2\alpha)K_1K_2K_3k_1N_T - 2N_TK_1K_2k_1k_2$$

$$A_7 = -(2+\alpha)K_1K_2K_3k_1k_2N_T$$

For specified temperature, total number density, types of gases, and relative percentages of each gas present, the above polynomial can be solved to yield the electron density, provided the partition functions are known. Once the electron density is known, all the particle densities can be calculated from Eqs. (3) and (4).

On the basis of Maxwell-Boltzmann statistics, the internal partition function of an atom or ion is

$$Q_i(n) = \sum_{n=n_L}^{n_c} g_i(n) \exp[E_i(n)/kT] \tag{7}$$

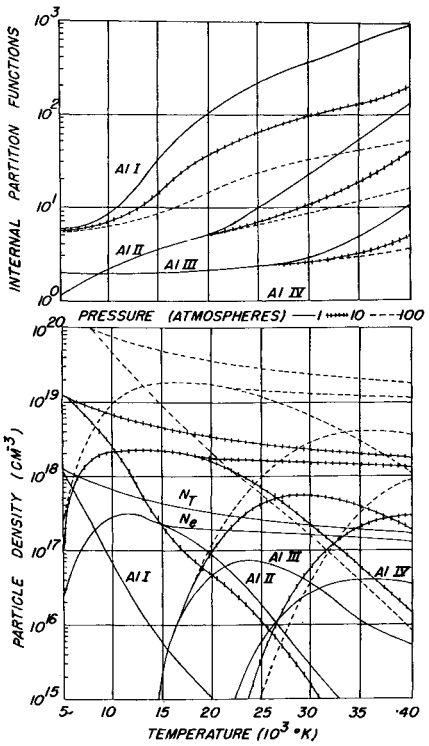

Fig. 2 Internal partition functions and compositions of pure aluminum plasma.

where $g_i(n)$ is the statistical weight of the nth energy level $E_i(n)$. The partition function series is summed theoretically over all values of the principal quantum number from the lowest possible value corresponding to the ground state energy level to the series terminating or cut-off principal quantum number n_c, corresponding to the lowered ionization potential in a plasma. The Debye shielding criterion was used to calculate the series terminating quantum number as[10]

$$n_c = 36.11 \times 10^3 \left[Z_{\text{eff}}^{2T} \Big/ \left(N_e + \sum_i^{N+M} Z_i^2 N_i \right) \right]^{1/4} \quad (8)$$

where Z_{eff} is the effective charge of the atom or ion. The effective charge was assumed to be one for atoms, two for singly charged ions, etc.

One difficulty encountered in the calculation of the internal partition functions was that energy terms in addition to those that have been observed experimentally[11] were needed in the computations. There was a significant lack of experimental data at the higher quantum numbers. Since these upper energy states are expected to contribute significantly to the values of the partition functions, it was necessary to estimate energy levels in some cases. A modified Rydberg extrapolation technique was used to estimate the missing energy levels for high quantum numbers of a fixed total configuration. The mixing terms were predicted by an equation of the form

$$E(n) = I - R/(n + \sum_{i=0}^{p} a_i n^{-i})^2 \quad (9)$$

where $R = 109{,}735\ \text{cm}^{-1}$ is the Rydberg number for aluminum. A computer program was used to evaluate the coefficients a_i in terms of known energy levels at the lower quantum numbers. The integer p was usually taken to be 4 or 5. Once the set a_i were found, the missing energy levels $E(n)$ could be determined as a function of the principal quantum number. It was also necessary to estimate energy levels for higher states of a given fixed principal quantum number. An atom and ion having the same number of orbital electrons form an isoelectronic sequence, all members of which exhibit similar spectra. The unobserved energy terms of one member of the isoelectronic sequence was estimated by comparison with the observed energy levels of other members of the sequence. For large values of the quantum number, the hydrogenic approximation

$$E(n) = I - I/n^2 \quad (10)$$

was employed in the calculations.

A computer program was developed to determine the equilibrium composition of aluminum and iron plasmas. Since the cut-off quantum number presupposes a knowledge of the particle number densities and vice versa, the composition calculations involve the iterative solution of the partition function equation, cut-off quantum number relation, electron density polynomial, and Saha equations. In order to start the iterative solution procedure, an initial value of the series cut-off quantum number was assumed, and then the partition functions and lowered ionization potentials were used to calculate the mass-action coefficients. By experience it was found that a cut-off quantum number of 20 was a good first estimate for neutral aluminum. The electron density and the heavy particle densities were determined using the assumed mass-action coefficients. The cut-off quantum number was then recomputed and compared with the assumed value. If the values were not the same, a new value was assumed and

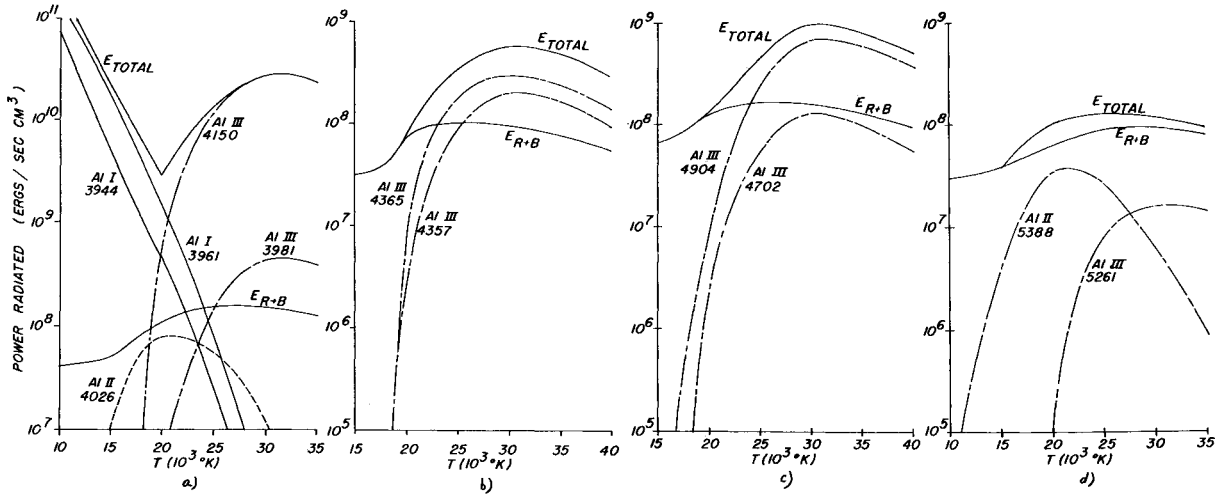

Fig. 3 Power radiated from a pure aluminum plasma in the four wavelength intervals: a) 3820–4200 Å, b) 4200–4450 Å; c) 4600–5050 Å; and d) 5200–5450 Å.

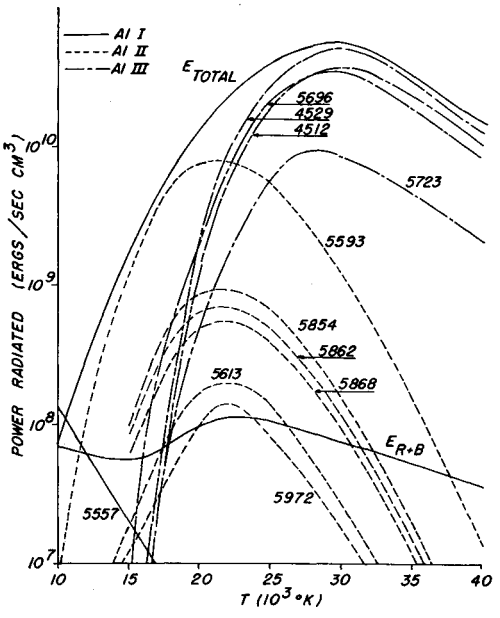

Fig. 4 Power radiated from a pure aluminum plasma in the interval 5570-5980 Å.

the iterative procedure was continued until the assumed and calculated values were the same. This method yielded the cut-off quantum number, internal partition function, and number density for each species.

Radiation from LTE, Optically Thin Metallic Plasma

Line Radiation

The power radiated per unit volume in the spectral line centered at the frequency ν is

$$P_z^L(\nu) = h\nu A_z(m,n)N_z(m)$$

where $A_z(m,n)$ is the probability that a transition will occur from energy level $E(m)$ into energy level $E(n)$, and $N_z(m)$ is the number density of radiators in energy level $E(m)$ of specie z. The excited state number density $N_z(m)$ is related to the total number density of the atom or ion by the Boltzmann equation $N_z(m) = (N_z/Q_z)g_z(m)\exp[-E_z(m)/kT]$ so that

$$P_z^L(\nu) = (h\nu/4\pi)(N_z/Q_z)g_z(m)A_z(m,n)\exp[-E_z(m)/kT] \quad (11)$$

is the total power radiated per unit volume per unit solid angle in the spectral line centered at the frequency ν.

Because of the interactions between the emitting atoms and ions in a plasma, the transitions will not occur at one precise energy or frequency, so that the energy in a given spectral line will be distributed about a given frequency (or wavelength). The spectral line is then said to be broadened and to possess a line shape or profile $L(\nu)$, such that the probability of emission in the frequency interval $d\nu$ is $L(\nu)d\nu$ where $\int L(\nu)d\nu = 1$. In addition to being broadened, the spectral line is shifted from the isolated atom wavelength. The effects of broadening were not included in the general over-all radiation energy analysis, but some approximate equations developed by Griem[8] were used to calculate the effects of broadening and shift for two groups of aluminum lines as discussed later. In the present radiation model, all the spectral line radiation was summed within a given wavelength interval, so that the total energy radiated in the unshifted and nonbroadened lines, as calculated using Eq. (11), is the same as for the shifted and broadened lines except for the lines near the end of the wavelength intervals. Measured transition probability data[14–20] were utilized where possible. To supplement the sparse measured data for aluminum, a few theoretical values calculated by Griem[8] were used.

Recombination Radiation

Recombination radiation occurs when an electron recombines with an ion to form an ion in a lower state of ionization z and a photon is emitted with energy $h\nu = I_z - E_z(n) + \frac{1}{2}m_e v_e^2$, where v_e is the electron velocity and $E_z(n)$ is the bound energy level of the recombined electron and ion. By requiring a balance between recombination and ionization events in equilibrium and relating the ionization cross sections to transition probabilities, the recombination radiation in the wavelength interval $d\nu$ per unit volume of the radiating source per unit solid angle is found to be[2,8,13]

$$P_z^R(\lambda)\,d\lambda = \frac{16e^4h(Z_{\text{eff}})N_eN_z}{3\pi(3)^{1/2}m_e^2c^2\lambda^2}\,[I_z/kT]^{3/2}\exp(-hc/\lambda kT)\times \sum_{n_{\min}}^{n_c}\frac{g_{fb}}{h^3}\exp\left[\frac{I_z - E_z(n)}{kT}\right]d\lambda \quad (12)$$

g_{fb} is the free-bound Gaunt factor (assumed to be unity in the calculations), n is the principal quantum number, and $n_{\min}$ is defined as

$$n_{\min} = n_c[I_z/(n_c^2h\nu + I_z)]^{1/2}$$

Equation (12) was derived for the case of hydrogenic atoms and ions. For nonhydrogenic atoms and ions, the recombi-

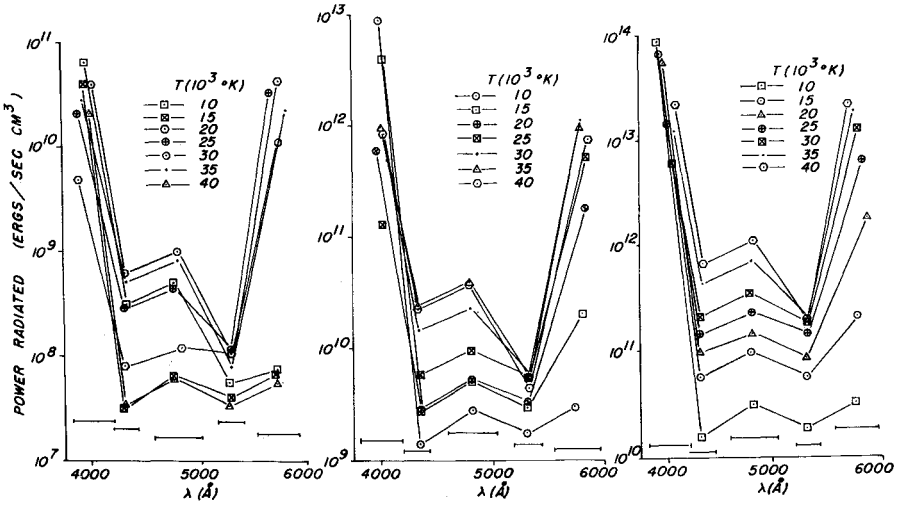

Fig. 5 Power radiated from a pure aluminum plasma at 1, 10, and 100 atm, respectively.

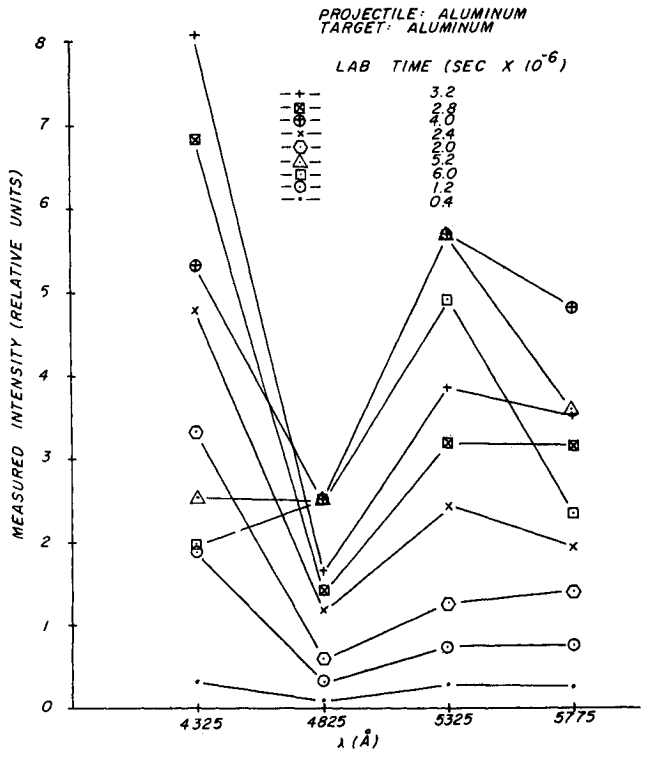

Fig. 6 Typical experimental results for aluminum-aluminum impacts.

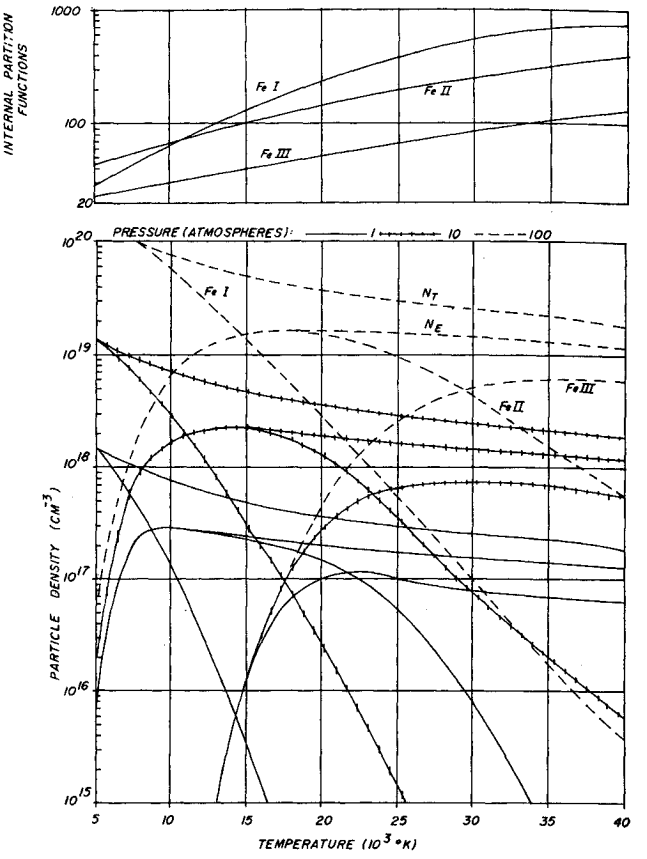

Fig. 7 Internal partition functions and compositions for pure iron plasma.

nation cross sections must be known. However, there were very little information and data available, so that the hydrogenic approximation should yield at least a good first estimate of the emitted energy due to recombination radiation.

Bremsstrahlung

Bremsstrahlung results when an electron makes a transition from one free energy state to another free energy state due to an encounter with another particle. In the present case, the major contribution to this type of radiation is due to electron-ion collisions. The bremsstrahlung contribution to the radiated power becomes[2,8]

$$P_z^B\, d\lambda = \frac{8e^4hZ_{\text{eff}}}{3\pi(3)^{1/2}m_e^2c^2}\frac{N_eN_z}{\lambda^2}(I_z/kT)^{1/2}\exp(I_z/n_c^2kT) \quad (13)$$
$$g_{ff}\exp(-hc/\lambda kT)d\lambda$$

where g_{ff} is the free-free Gaunt factor (which was assumed to be one in the calculations).

Numerical Results for Aluminum Plasma

For total pressures of 1, 10, and 100 atm and temperatures (T) between 5000° and 40,000°K, spectral line radiation, recombination radiation, and bremsstrahlung were calculated for the wavelength interval of the experiments of Reid, Harwell, and Hughes.[2] The total power radiated was then calculated for four wavelength bands corresponding to the normalized spectral widths of the experimental band pass filters.[2]

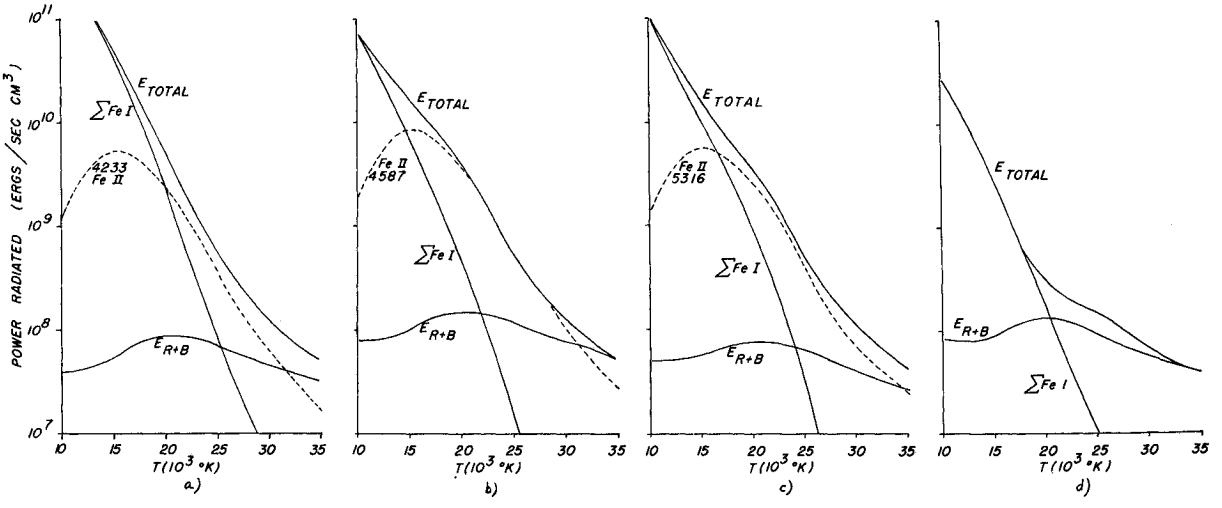

Fig. 8 Total power radiated from a pure iron plasma at 1 atm in the wavelength intervals a) 4200–4450 Å, b) 4600–5050 Å, c) 5200–5450 Å, and d) 5570–5980 Å.

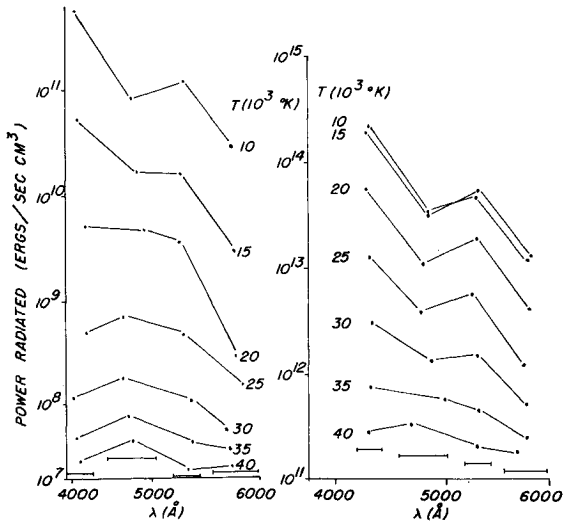

Fig. 9 Power radiated from a pure iron plasma at 1 atm and 10 atm, respectively.

The internal partition functions and compositions calculated for a pure aluminum plasma are presented in Fig. 2. The partition function increases with T as the higher bound energy states are populated. For AlIV, it is essentially constant for the temperature range considered.

The total energy radiated from a unit volume of plasma per unit time per unit solid angle was calculated for the wavelength intervals 4200–4450 Å, 4600–5050 Å, 5200–5450 Å, and 5570–5980 Å corresponding to the wavelength intervals of filters utilized in the experiments.[2] Since there are several significant spectral lines of aluminum in the interval 3820–4200 Å, numerical calculations were also carried out for this wavelength interval, even though it does not correspond to an experimental one. For purposes of discussion, the 1-atm case will be chosen to describe the pertinent details of the line and continuum radiation results. The results of the computations are presented in Figs. 3–5. Similar results were obtained at pressures of 10 and 100 atm.

For the first wavelength interval (3820–4200 Å), as shown in Fig. 3a, at $T < 20{,}000°$K, the radiation is predominately that due to line radiation from neutral aluminum (AlI). The power radiated at 3944 Å and 3961 Å is one to three orders of magnitude greater than that due to continuum radiation for $T < 20{,}000°$K. The total radiated power decreases as temperature increases for $T < 20{,}000°$K, because the number of radiating neutral atoms decreases (Fig. 2). As T continues to increase, the relative importance of the AlI spectral lines is diminished, while the significance of the singly ionized (AlII) and doubly ionized (AlIII) spectral lines increases. For the wavelength interval being considered, AlII had only one significant spectral line at 4026 Å for which transition probability data were available. The AlIII spectral lines 3981 Å and 4150 Å dominate the radiation behavior above 20,000°K. Throughout the entire temperature range, the continuum radiation is almost negligible compared to the line radiation.

As indicated in Fig. 3b for the wavelength interval 4200–4450 Å, the emitted radiation is due principally to recombination radiation and bremsstrahlung below 25,000°K, since there were no significant AlI or AlII spectral line data available for this wavelength interval. Above 25,000°K, the radiation is primarily that of AlIII spectral line radiation at 4357 Å and 4365 Å. In a similar manner, the radiation in the interval 4600–5050 Å (Fig. 3c) is primarily continuum radiation below 25,000°K and AlIII line radiation at 4702 Å and 4904 Å above this temperature. Radiation at 4998 Å (AlII) was negligible for all temperatures considered. The total radiation in the fourth wavelength interval 5200–5450 Å (Fig. 3d) is primarily continuum radiation with relatively

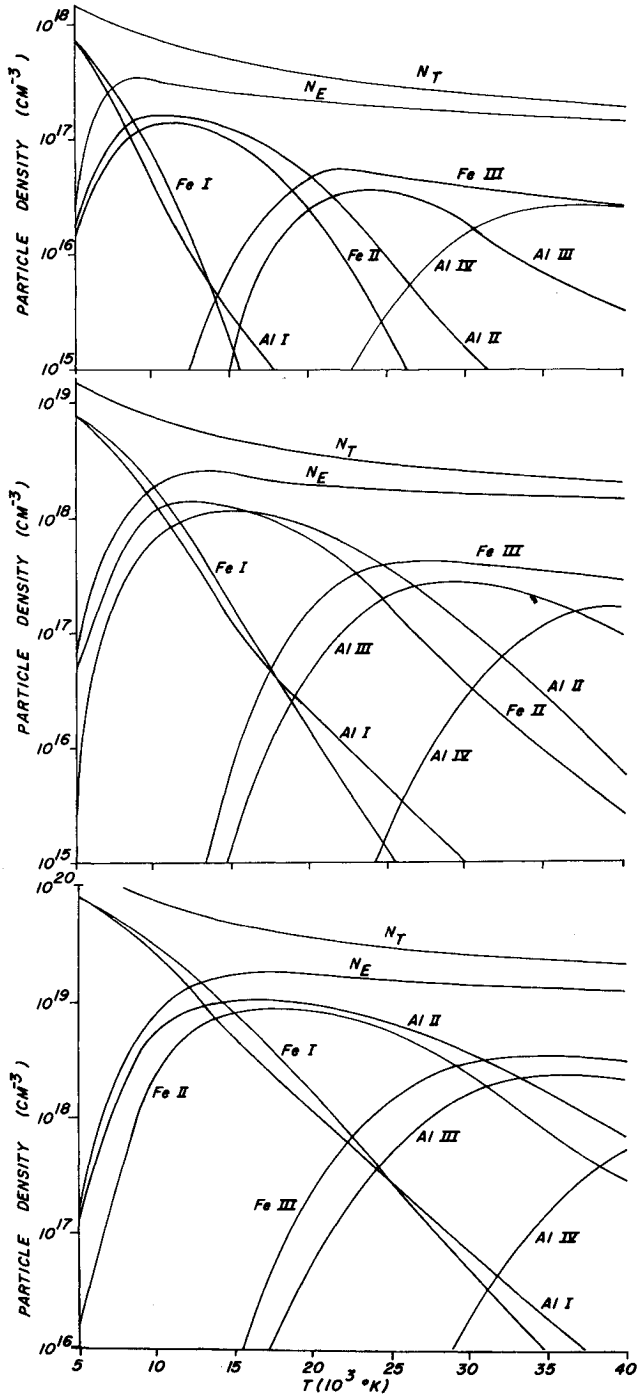

Fig. 10 Compositions of aluminum-iron plasma at 1, 10, and 100 atm, respectively.

small contributions from the AlII spectral line 5388 Å between 15,000°K and 30,000°K and the AlIII spectral line 5261 Å between 25,000° and 40,000°K.

In the fifth wavelength interval, 5570–5980 Å (Fig. 4) line radiation predominates. There are several strong AlII spectral lines. The most significant one is located at 5593 Å. Above 25,000°K the AlIII spectral lines 5696 Å and 5723 Å provide most of the radiation. For completeness, it should be observed in Fig. 4 that there are significant spectral lines outside the five wavelength regions. AlI has two relatively strong lines at 5557 Å and 5558 Å, which may be significant at low temperatures. AlIII lines at 4529 Å and 4512 Å are significant contributors to the radiation above 20,000°K.

In order to visualize the relative significance of the power radiated in the five wavelength intervals, the total power

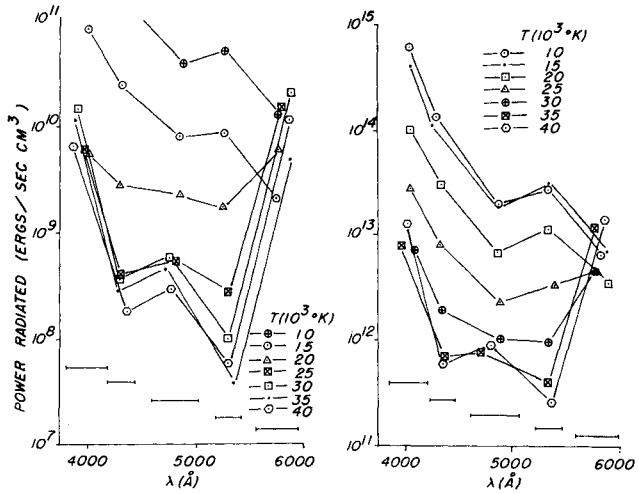

Fig. 11 Power radiated from an aluminum-iron plasma at 1 and 100 atm, respectively.

radiated is presented in Figs. 5a, b, and c as a function of λ for pressures of 1, 10, and 100 atm, respectively. The various wavelength intervals are connected by straight lines, not to indicate radiation variation between the various intervals, but merely to connect the common temperature values.

Comparison of Theory and Previous Experiments, Aluminum-Aluminum

Typical experimental results obtained by Hull[2] for aluminum-aluminum impacts are presented in Fig. 6. Curves of spectral distribution, at specified temperature and pressure, can be selected from the theoretical results that agree qualitatively with the general temporal behavior observed in the experiments. Only the spectral distribution has any meaning in this comparison. The mathematical model predicts the power radiated from a unit volume of plasma. Since there was no way to determine the radiating volume of the experimental plasma source, a comparison of the magnitudes was not meaningful.

For the pure aluminum case, it would appear that there is no agreement between the experimental data (Fig. 6) and the theoretical calculations (Fig. 5). However, if the pressure is sufficiently high, there could be enough broadening and shift of the strong spectral lines below 4200 Å to increase the power radiated in the wavelength interval 4200–4450 Å above that of the 4600–5050 Å interval. Approximate broadening equations developed by Griem[8] were used to calculate the broadening and shift of two groups of aluminum lines (3944–3961 Å and 5557 Å) for pressures of 1, 10, and 100 atm. The most prominant ones, 3944 and 3961 Å, have line half-widths of about 10 Å and 100 Å and line shifts of 5 Å and 50 Å for pressures of 10 and 100 atm, respectively. The lack of over-all agreement may also be due to the manner in which the experimental data were corrected for photomultiplier response and filter attenuation of the emitted radiation. The filter response factors were assumed to be flat-topped[2] with a sharp cut-off at the wavelength edges of the transmission region. However, there was some radiated power transmitted in the wings of the filter bands, e.g., the filter for the wavelength interval 4200–4450 Å transmitted some radiation in the wavelength region below 4100 Å.[2] Since the radiation at the wavelengths 3944 Å and 3961 Å is many orders of magnitude larger than from the other known lines, even a small transmission factor of the filter would allow a considerable amount of the radiation to be detected by the photomultipliers. If only a small part of the power radiated in the first wavelength interval of Fig. 5 is put into the second interval, the radiated power in the second interval could then be larger than that in the third interval. Similarly, a shift of the strong AlIII lines from the third interval would lead to a significant decrease in radiated power in the third interval and an increase in the fourth interval. Since the line shift at long wavelengths is much larger than at short wavelengths, some of the lines in the fifth interval would be shifted outside the range of detectability of the photomultiplier. Possible qualitative agreement could be achieved in this manner; however, since the pressure broadening and line shifts are vital to this argument, and since they were not included in the theoretical calculations, no further attempt was made to resolve the lack of agreement.

It should be emphasized that the experimental projectiles and targets were not pure metals. The aluminum projectiles contained 3.8–4.9% Cu, 1.2–1.8% Mg, and several other impurities. Copper has several strong spectral lines in wavelength bands where there were no aluminum line data. This may be one possible explanation for the disagreement between the theoretical calculations for aluminum and the experimental data.

Numerical Results for Pure Iron Plasma

Calculated internal partition functions and compositions are presented in Fig. 7. Since the partition function series for pure iron was summed over all observed energy levels, the internal partition function for iron did not change with pressure. The results of the calculations of total power radiated are presented in Figs. 8 and 9. For all wavelength intervals

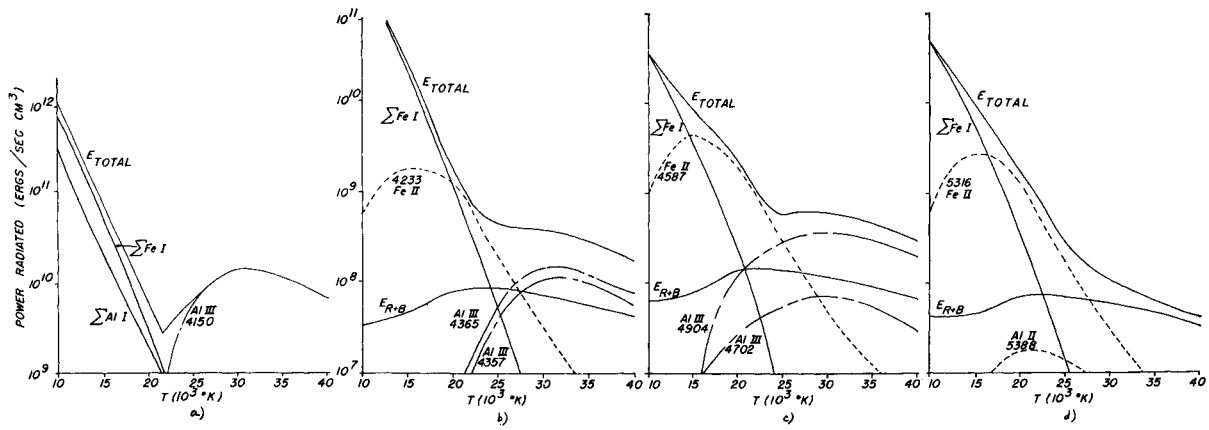

Fig. 12 Power radiated in the wavelength intervals a) 3820–4200 Å, b) 4200–4450 Å, c) 4600–5050 Å, and 5200–5450 Å.

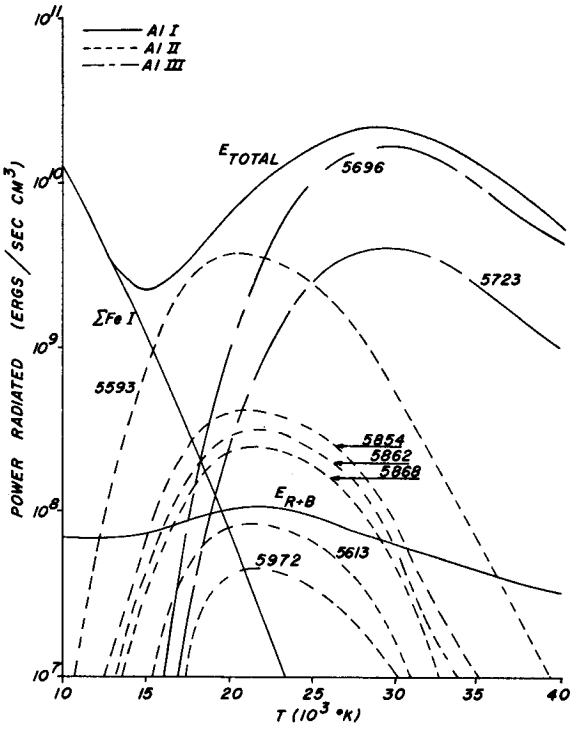

Fig. 13 Power radiated in the wavelength interval 5570–5980 Å from an aluminum-iron plasma.

the dominant source of radiation for low temperatures is line radiation from the neutral iron (FeI) atoms. The total line radiation included contributions from 211 lines of FeI and 3 lines of FeII. There were no available transition probability data for FeIII. In the wavelength interval 4200–4450 Å, the FeII 4233 Å line radiation is larger than the FeI radiation for $T > 20{,}000°\text{K}$. In the range $15{,}000° \leq T \leq 30{,}000°\text{K}$, the predominant source of radiation in the wavelength intervals 4600–5050 Å and 5200–5450 Å is that of FeII line radiation at 4587 Å and 5316 Å, respectively. Above 30,000°K the dominant type of radiation appeared to be continuum radiation. However, there were no available transition probability data for FeIII, so that this may not actually be the case when data become available.

Numerical Results for Aluminum-Iron Plasma

For plasmas with equal numbers of aluminum and iron particles, the internal partition functions were essentially the same as those for the pure iron and pure aluminum cases. The results of the number density calculations are presented in Fig. 10.

The spectral distribution of the energy radiated from an aluminum-iron plasma is presented in Fig. 11 for pressures of 1 and 100 atm. Comparison of Fig. 11 with the corresponding figures for the pure metallic plasma cases shows that the shapes of the spectral distribution curves are similar to the pure iron case at low temperatures and to the pure aluminum case at the higher temperatures. This effect is shown more dramatically in Figs. 12 and 13; it may be due principally to the fact that there are many more lines available for FeI than for AII and that the effect of aluminum is not really significant until the AlIII spectral line contributions become large at $T > 20{,}000°\text{K}$.

For the first wavelength interval (3820–4200 Å) of Fig. 11a plotted as a function of temperature in Fig. 12a, the total radiation in the first interval, $E_T(1)$, for $T < 20{,}000°\text{K}$ is that due to line radiation from AII and FeI. The FeI line radiation is about a factor of two larger than the AII radiation at the lower temperatures. Above 20,000°K the AlIII spectral lines at 3981 Å and 4150 Å produce most of the total radiation. The characteristic behavior of $E_T(1)$ with temperature is similar to that of the pure aluminum case in spite of the large FeI contribution.

As indicated in Fig. 12b, at low temperatures, the energy radiated in the second wavelength interval $E_T(2)$ is predominantly that from FeI line radiation. Between 20,000 and 25,000°K, the FeII spectral line at 4233 Å becomes the predominant source of radiation. Above 25,000°K, the AlIII spectral lines at 4357 Å and 4365 Å furnish most of the radiation. As is the case of the second interval, $E_T(3)$, as shown in Fig. 12c, is due mostly to FeI line radiation at $T < 15{,}000°\text{K}$, to the FeII 4587 Å spectral line for $15{,}000° \leq T \leq 25{,}000°\text{K}$, and to AlIII spectral lines at 4702 Å and 4904 Å for $T > 25{,}000°\text{K}$. The continuum radiation is also significant in this wavelength interval. The situation is virtually the same for the fourth interval. As presented in Fig. 12d, $E_T(4)$ is primarily FeI line radiation up to 15,000°K, mostly 5316 Å FeII line radiation from there to 25,000°K, and continuum radiation at $T > 25{,}000°\text{K}$. For the fifth wavelength interval, $E_T(5)$ is presented in Fig. 13. Except for $T < 15{,}000°\text{K}$, the radiation is primarily that from the aluminum constituents.

Comparison of Theory and Previous Experiments

Experiments were carried out by Hull[2] for iron-iron, iron-aluminum, and aluminum-iron impacts. In an attempt to correlate the experimental data with the theoretical model, it became obvious in most cases for steel-steel impacts that the measured intensities in all four wavelength intervals (cen-

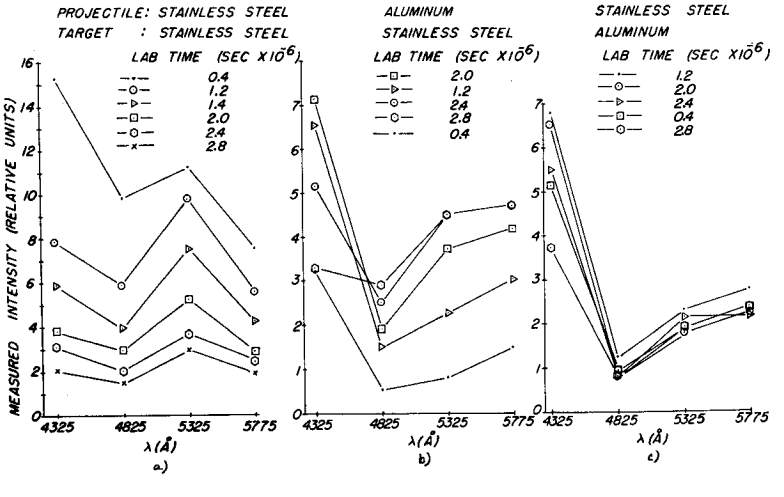

Fig. 14 Experimental spectral distributions for a) stainless steel-stainless steel, b) aluminum-stainless steel, and c) stainless steel-aluminum impacts.[2]

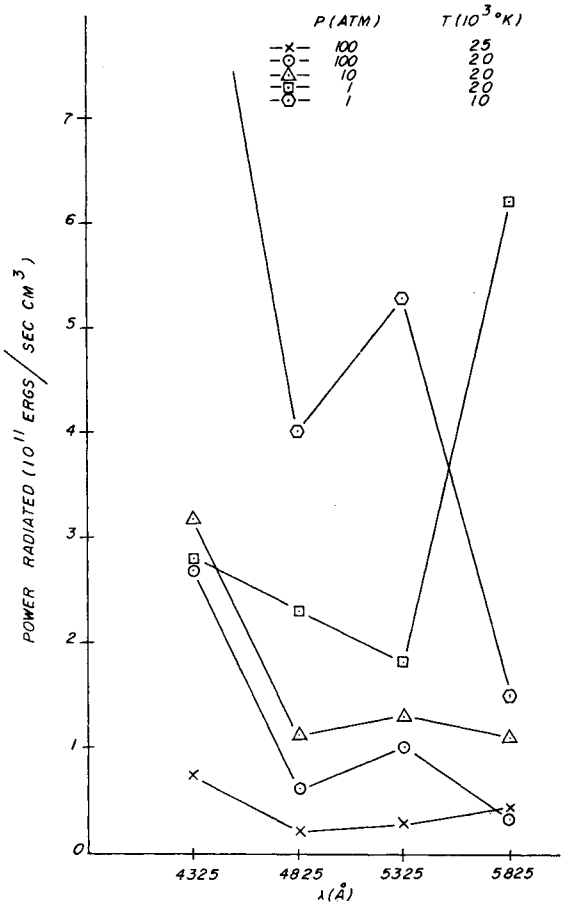

Fig. 15 Calculated spectral distribution for aluminum-iron plasma.

tered at 4325 Å, 4825 Å, 5325 Å, and 5825 Å) decrease with time after an extremely short time interval (<0.4 μsec in the case of Fig. 14a). It can be seen from Fig. 14a that the power radiated in the wavelength interval centered at 4325 Å is initially much larger than that of the other intervals and decreases rapidly with time. An attempt was made to determine whether similar curves could be found from the theoretical results that would qualitatively agree with the temporal behavior of Fig. 14a. A comparison of Figs. 9b and 14a indicates that there is qualitative agreement if the temperature is low ($\sim 10^4$ °K or less) or the pressure is high.

For the mixed case (aluminum-steel and steel-aluminum), the theoretical curves of Fig. 15 (selected from the theoretical results) qualitatively agree with the experimental data presented in Figs. 14b and 14c. This simply means that curves of similar shape could be found in both the experimental and theoretical results.

Conclusions

Qualitative agreement between the spectral distribution calculated for a pure aluminum plasma and the experimental values for aluminum-aluminum impacts was not achieved. Some qualitative agreement could be inferred if the plasma pressures were high enough to lead to considerable line shift and broadening. In addition, impurities in the experimental material could produce enough radiation to alter the over-all distribution of radiated power.

Some qualitative agreement between the spectral distribution calculated for a pure iron plasma and the experimental values for an iron-iron impact was attained. Comparison of the calculated results for the aluminum-iron case with the experimental data for aluminum-iron and iron-aluminum impacts indicated that agreement could be achieved if the plasma pressures were quite high. For high pressures, inclusion of line shift and broadening in the analytical model could lead to better qualitative agreement.

Even though these calculations were carried out for optically thin LTE metallic plasmas, they should provide data which will assist in the understanding of the impact flash produced in hypervelocity impacts. Improvements in the model such as the inclusion of more elements and the effects of pressure broadening and line shift are planned which should lead to better agreement between theory and experiment.

References

[1] Rollins, T. and Jean, B., "Radiation From Hypervelocity-Impact Generated Plasma," AIAA Paper 69-364, Cincinnati, Ohio, 1969.

[2] Reid, J. L., Harwell, K. E., and Hughes, A. R., "Theoretical and Experimental Investigation of the Relationship of Impact Flash to Physical Damage," TR AFATL-TR-67-138, Oct., 1967, Air Force Armament Lab., Eglin Air Force Base, Fla.

[3] MacCormack, R. W., "Investigation of Impact Flash at Low Ambient Pressures," *Proceedings of the Sixth Hypervelocity Impact Symposium*, Firestone Tire and Rubber Co., Cleveland, Ohio, Vol. II, 1963, p. 613.

[4] Koehler, R. A., "Spectroscopic Study of the Impact Flash," M. Sc. thesis, 1965, Univ. of Western Ontario.

[5] Jean, B. and Rollins, T., "Hypervelocity Impact Flash for Hit Detection and Damage Assessment," TR AFATL-TR-68-46, 1968, Air Force Armament Lab., Eglin Air Force Base, Fla.

[6] Jean, B., "Experimental Observations of Optical Radiation Associated with Hypervelocity Impact," *AIAA Journal*, Vol. 4, No. 10, Oct. 1966, pp. 1854–1856.

[7] Griem, H. R., "Validity of Local Thermal Equilibrium in Plasma Spectroscopy," *Physical Review*, Vol. 131, No. 3, 1963, pp. 1170–1176.

[8] Griem, H. R., *Plasma Spectroscopy*, McGraw-Hill, New York, 1964.

[9] McWhirter, R. W. P., "Spectral Intensities," *Plasma Diagnostic Techniques*, edited by R. H. Huddlestone and S. L. Leonard, Academic Press, New York, 1965, pp. 201–264.

[10] Drellishak, K. S., Knapp C. F., and Cambel, A. B, "Partition Function and Thermodynamic Properties of Argon Plasma," *The Physics of Fluids*, Vol. 6, No. 9, Sept., 1963, pp. 1280–1288.

[11] Moore, C. E., "Atomic Energy Levels," Circular 467, Vol. I, 1949, Vol. II, 1952, National Bureau of Standards, Washington, D.C.

[12] Cooper, J., "Plasma Spectroscopy," *Reports on Progress in Physics*, Vol. 29, 1966, American Institute of Physics, New York, pp. 35–130.

[13] Corliss, C. H. and Bozman, W. R., "Experimental Transition Probabilities for Spectral Lines of Seventy Elements," Monograph 53, 1962, National Bureau of Standards, Washington, D.C.

[14] Allen, C. W., *Astrophysical Quantities*, Athlone Press, London, 1963, pp. 70, 72, and 76.

[15] Goldberg, L., Muller, E. A., and Aller, L. H., "Abundances of Elements," *Astrophysical Journal Supplement*, Vol. 5, 1960, pp. 19, 20, and 30.

[16] Dickerman, P. J. and Devel, R. W., "Measurement of Relative Transition Probabilities for Some Lines of the CaI, AlI, and MoI Spectra," *Journal of Quantitative Spectroscopy and Radiative Transfer*, Vol. 4, 1964, pp. 807–817.

[17] Allen, C. W., "Absolute Oscillator Strength Measurements in Mg, Ca, and Atoms," *Monthly Notices*, Vol. 117, 1957, Royal Astronomical Society, pp. 622–628.

[18] Eddy, J. A., House, L. L., and Zirin, H., "Oscillator Strength for $3s\,3p^2\ {}^2S\ 3s^2\,3p\ {}^2P$ Transition in AlI," *Astrophysical Journal*, Vol. 131, 1961, pp. 299–302.

[19] Megger, W. F., Corliss, W. H., and Scribner, B. F., "Tables of Spectral Line Intensities," Monograph 32, 1961, National Bureau of Standards, Washington, D.C.

[20] Allen, C. W., "Oscillator Strengths of Neutral Atoms of the Iron Groups," *Monthly Notices*, Vol. 121, 1960, Royal Astronomical Society, p. 299.